

Effects of the Graphene Additive on the Corrosion Resistance of the Plasma Electrolytic Oxidation (PEO) Coating on the AZ91 Magnesium Alloy

Baojun Han^{1,2,*}, Yang Yang^{1,2}, Jing Li², Hao Deng², Chubin Yang^{1,2}

¹ Jiangxi Provincial Engineering Research Center for Magnesium alloys, Gannan Normal University, Ganzhou 341000, China

² School of Chemistry and Chemical Engineering, Gannan Normal University, Ganzhou 341000, China

*E-mail: baojunhan@126.com

Received: 28 May 2018 / *Accepted:* 29 June 2018 / *Published:* 5 August 2018

Graphene was added into the electrolyte during the preparation of plasma electrolytic oxidation (PEO) coating on the AZ91 Mg alloy. The effects of graphene additive on the surface morphology, phase composition and chemical composition of the PEO coating were characterized by scanning electron microscopy (SEM), X-ray diffraction (XRD) and X-ray photoelectron spectroscopy (XPS). Additionally, the effect of the graphene additive on the mechanical property of the PEO coating was evaluated using micro-hardness tester. Furthermore, the corrosion resistance of the coatings was tested by the potentiodynamic polarization curves and the electrochemical impedance spectroscopy (EIS). The results show that the graphene was successfully added into the PEO coating, and the incorporation of graphene reduced the number and size of micro-pores and cracks in the coating. Compared with the AZ91 Mg substrate, the micro-hardness of the PEO coating increased more than 15 times, and the corrosion current density decreased about three orders of magnitude when the amount of graphene addition in the electrolyte was 250 mg/L.

Keywords: AZ91 Mg alloy, plasma electrolytic oxidation (PEO), graphene, corrosion resistance, micro-hardness

1. INTRODUCTION

Magnesium (Mg) is the lightest of all metals used as the basis for constructional alloys, and Mg alloys are widely used in many fields such as aerospace engineering field, communication industry and implant materials because it possesses excellent properties such as high strength to weight ration, high

specific strength, good casting ability, excellent electromagnetic shielding characteristic and favorable bio-compatibility [1-3]. However, high chemical activity and poor corrosion resistance of Mg alloys seriously limit their further applications, especially in some aggressive environments [4,5]. The surface treatment is the most effective and direct method to improve the corrosion resistance of Mg alloys. There are several surface treatment techniques proposed for protection of Mg alloys. These techniques include chemical conversion coating [6], anodizing [7], physical vapor phase deposition [8], the electroplating [9] and the plasma electrolytic oxidation (PEO) [10]. Among them, the PEO is believed to be one of the most effective methods to protect Mg alloys because the bonding strength is firm, and the electrolytes are environmentally friendly [11,12].

Unfortunately, the PEO coating is porous, so it can not provide long-term protection for the substrate [13-15]. Over the past few decades, addition of particles into the PEO electrolytes has been explored as new strategy to provide a wider range of chemical composition and enhanced the compound properties of the PEO coatings [16]. These added particles can be incorporated into the PEO coatings during the processing, which will result in obtaining a compact coating. The effect of addition of SiC nanoparticles on the microstructural, tribological and electrochemical properties of the PEO coating on AZ31 Mg alloy was studied by Nasiri Vatan et al., and they found that the friction coefficient and wear rate of SiC-containing coating are much lower than the uncoated AZ31 Mg alloy and the SiC-free coatings [17]. Lu et al. [18] obtained the photo-catalytic active PEO coating on AM50 Mg alloy by adding the TiO₂ particles into the electrolyte using lower voltage and long processing time. Mashtalyar et al. [19] fabricated the protective and multifunctional coatings on MA8 Mg alloy by PEO with addition of nano-sized titanium nitride particles into the corresponding electrolyte, and found that the micro-hardness of the coating with the nanoparticle concentration of 3 g/L increased twofold. Stojadinović et al. [20] reported the MgO/ZnO photo-active PEO coatings on AZ31 Mg alloy was obtained with ZnO particles addition in the electrolyte. It was found that the addition of ZnO particles do not significantly influence the surface morphology of the coating, but its photo-luminescent emission spectra sharp band was centered at about 380 nm and broad band was centered at about 535 nm, and the photo-activity of obtained coatings increased with processing time.

Graphene, a new discovered carbon allotrope, and which was first isolated by simple mechanical exfoliation in 2004. It is a kind of two dimensional honey comb single layer crystal lattice formed by the tightly packed sp² bonded carbon atoms. The graphene possesses excellent electrical properties, highest thermal conductivity and extraordinary mechanical properties [21-23]. The extraordinary properties of graphene make it become an effective barrier toward oxidation and corrosion of a substrate [24]. However, there are few reports about using graphene in coating fields published in recent years. Prasai et al. [25] fabricated the graphene coating on copper and nickel either by chemical vapor deposition or just by mechanically transferring, and the results demonstrated that the graphene coatings apparently inhibit the corrosion rate of copper and nickel. Selvam et al. [26] investigated the electrochemical corrosion behavior of graphene coated Mg in salt electrolytes of Na₂SO₄, NaCl and KCl etc., and the results indicated that its corrosion rate drastically drops when the Mg was coated with thin layer graphene. Singh et al. [27] fabricated a robust composite coating reinforced by graphene using method of aqueous cathodic electro-phoretic deposition, and found that the coating has excellent corrosion

resistance. Zhao et al. [28] prepared a PEO coating on AZ31 Mg alloy by adding graphene oxide (GO) into the electrolyte and the results indicated that the GO successfully incorporated into the PEO coating.

In coating applications, graphene is believed to be promising but the articles designated for coating applications are limited. In present investigation, the PEO coating on the AZ91 Mg alloy was fabricated in electrolytes containing different concentrations of graphene. The surface morphology, phase composition and chemical composition of the PEO coating were characterized by scanning electron microscopy (SEM), X-ray diffraction (XRD) and X-ray photoelectron spectroscopy (XPS). Furthermore, the effect of the addition of graphene on the corrosion resistance and mechanical property of the PEO coating was evaluated using electrochemical station and micro-hardness tester.

2. EXPERIMENTAL PROCEDURE

2.1 Materials and experimental process

The substrate material used in present investigation was AZ91 Mg alloy, and which chemical compositions were as listed in Table 1. The samples were firstly cut into cubic with dimension of 10 mm × 10 mm × 10 mm, and then were grounded up to 1500 grits using silicon carbide abrasive papers. Followed by PEO processing, the samples were ultrasonically rinsed with acetone for 15 min, distilled water and dried in the air at room temperature.

Table 1. Chemical compositions of the AZ91 Mg substrate.

Element	Al	Zn	Mn	Si	Fe	Cu	Mg
Content (wt%)	8.95	0.93	0.21	0.011	0.08	0.01	Balance

The graphene additive used in the present investigation was produced by the MORSH Technology Co. Ltd of Ningbo City, China. Fig.1 shows the SEM morphology of the graphene additive, and Fig. 2 shows the corresponding Raman spectrum. It can be found in Fig. 2 that peaks at approximately of 1347 cm^{-1} , 1585 cm^{-1} and 2670 cm^{-1} are detected, which are usually called D, G and 2D bands of graphene, respectively [29].

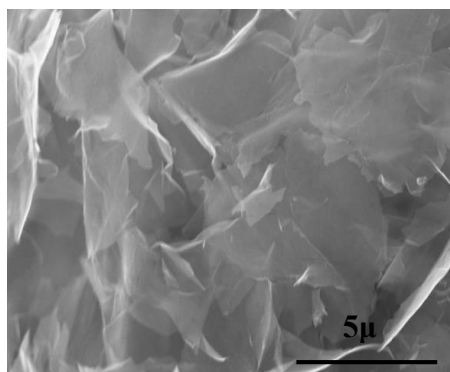


Figure 1. Typical SEM morphology of the graphene used in present research

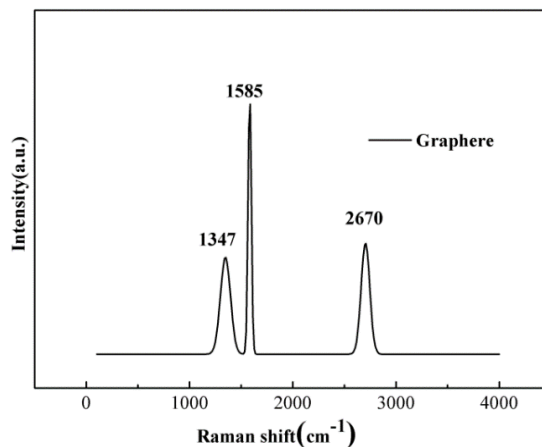


Figure 2. Typical Raman spectrum of the used graphene additive

A 30KW DC pulse power supply (WHD30, China) equipped with an electrolyte cooling system was used for PEO processing. The specimens were used as the anode and the 316L stainless steel bath was used as the cathode. The PEO processing was conducted with the electrolyte temperature maintained at 25-35 °C and during which processing the electrolyte was persistently stirred with compressed air bubbles.

The alkaline electrolytes containing 6 g/L potassium hydroxide (KOH), 20 g/L sodium silicate (Na₂SiO₃·9H₂O), and 0, 50 mg/L, 150 mg/L and 250 mg/L graphene were prepared. All the chemical reagents used were referred to analytical reagent (AR) grade. Before processing, the electrolytes were ultrasonically dispersed for 30 min with the purpose to make the graphene be homogeneously suspended. Based on many pretrials, the parameters utilized in present investigation were as listed in Table 2. After the PEO processing, the samples were firstly washed in ethanol, and then in distilled water and dried in the air at room temperature at last.

Table 2. PEO processing parameters utilized in present study.

processing Parameters	positive voltage	negative voltage	processing frequency	dutcy cycle	Duty ratio	processing time
Value	480 V	30 V	500Hz	10%	1:1	10 min

2.2 Characterization of the Coatings

A digital thickness gauge (Time, TT230) was used to measure the thickness of the PEO coating, and the average of 10-point measurements was utilized. A micro-hardness tester (Shimadzu, HMV-21GST) was used to test the surface micro-hardness of the coating, and the load of 1kg and holding time 50 s was set. The average of 5-point micro-hardness measurements was used in the present work. The cross section and surface morphology of the coatings were observed using scanning electron microscopy (SEM, Quanta, FEI450), and at the same time, energy dispersive spectroscopy (EDS, Oxford) attached to the SEM and the X-ray photoelectron spectroscopy (XPS, ThermoFisher Scientific, ESCALAB

250Xi) with an Al K α ($h\nu=1486.6\text{eV}$) monochromatic source were used to analyse the chemical composition of the coatings. The X-ray diffraction (XRD, Bruker, D8 ADVANCE) with Cu K α radiation ($\lambda=0.154060\text{nm}$) over an angle range of $10\sim 90^\circ$ (2θ values) was utilized to identify the phase composition of the coating.

The potentiodynamic polarization curves and the electrochemical impedance spectroscopy (EIS) measurements were used to test the corrosion resistance of the coatings in a 3.5% NaCl solution by an electrochemical workstation (Metrohm, PGSTA302A) equipped with a three-electrode cell system. The three-electrode cell system comprised a reference electrode (a saturated calomel electrode), a counter electrode (a platinum foil) and a working electrode (samples). The surface area of the working electrode was set as 1.0 cm^2 . The specimens were immersed in the 3.5 wt.% NaCl solution at room temperature for 30min to attain a steady state of the open circuit potential prior to the electrochemical tests, and at least three independent measurements were conducted under every experimental condition. The EIS measurements were executed at open circuit potential with a frequency range of 10^{-2} Hz to 10^5 Hz . The dynamic polarization curves were performed at a scanning rate of 1 mV/s from -0.2 to 0.3V with respect to the open circuit potential. The corrosion potential (E_{corr}) and corrosion current density (i_{corr}) etc. were fitted by the Tafel extrapolation method[30-32].

3. RESULTS AND DISCUSSION

3.1 Current variation with time curves under constant voltage

The variation of current with processing time at constant voltage with and without graphene addition is shown in Fig. 3. It can be seen that samples coated with PEO coatings showed very good sameness in the curves shape, i.e. the current sharply decreased and then gradually decreased with time during the PEO processing. The results are similar to the others investigations [33-35], a typical three-stages can be found according to current variations versus time curves, although the discharges could not be observed visually due to the opacity of the electrolyte suspension. During the first stage, the current decreased linearly with time, and which can be corresponded to the conventional anodizing. In the second stage, the slope of current varying with time decreased, and this corresponds to the formation of a nonuniform PEO coating. The obtained PEO coating will increase the electric resistance, and decrease the current. During the third stage, the slope is approximately zero based on the reason that a compact and uniform coating with large electric resistance were formed. Whereas, Fig. 3 also shows that the addition of graphene affects the evolution of the current during the whole process, and graphene containing coating have lower sparking current in comparison to sample coated in electrolyte without additives. This can be attributed to the addition of graphene in electrolytes may result in much more compact and uniform coating with higher electrical resistance, therefore to maintain voltage constant, lower current density is demanded [36,37]. It also could be found that the current density versus time curves of samples containing graphene are much more uniform and with less fluctuations, showing more uniform formation of coating during PEO processing.

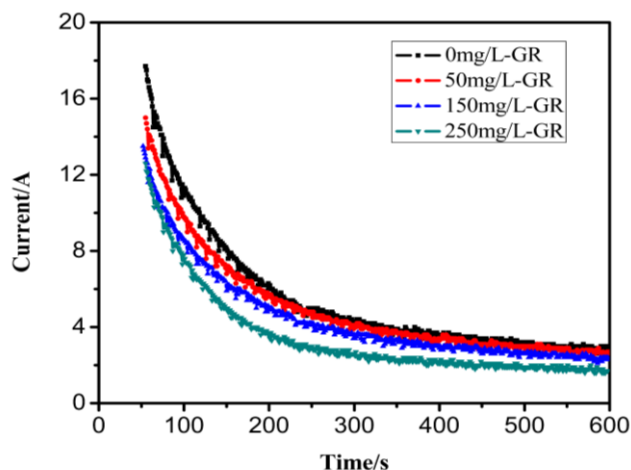


Figure 3. Current variation with time curves of the samples processed by PEO with 480 V positive voltage and 30 V negative voltage in the electrolytes added with different amounts of graphene

3.2 Thickness and micro-hardness analysis of the coatings

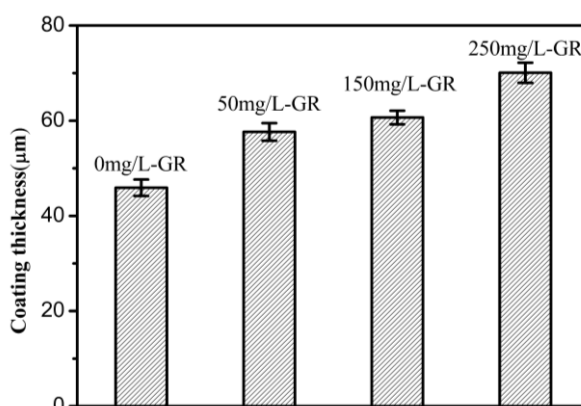


Figure 4. Thickness of the coatings processed in electrolytes added with different amounts of graphene

Fig. 4 shows the thickness values of the coatings processed in electrolytes containing different graphene addition. It is evident that with the introduction of graphene, the coatings thickness increases. Similar result has been reported by Apelfeld et al. [38], in which they claimed that the addition of nanozirconia increased the PEO coating thickness. The graphene additive accelerates the growth and contribute to obtain a denser and ticker PEO coating, which also has been proved by the decreasing current (Fig. 3). It also could be concluded from Fig. 4 that the samples coated with graphene additive in the electrolytes displayed lower standard deviation in the coatings thickness measurement , indicating the uniformity of the coatings .

Fig. 5 indicates the micro-hardness of AZ91 Mg alloy substrate, as well as PEO samples with and without graphene additives. It is apparently that the PEO treatment can obviously improve the micro-hardness and improve the abrasive performance of the substrate. Compared with the micro-hardness increasing reported in Reference [11] etc., to our knowledge, the micro-hardness enhancement in present investigation is the most evident one. The micro-hardness of the AZ91 Mg alloy substrate is only 52 HV. It is easily found that PEO coating without graphene can apparently improve the surface abrasive

performance of the substrate, and the micro-hardness value is up to 350 HV. Fig. 5 also indicates that the micro-hardness values of the PEO coatings increased with increasing graphene additive. When the graphene additive amount in the electrolyte was up to 250 mg/L, the micro-hardness of the coating is 808 HV, and which is much higher than the one without graphene additive, and the micro-hardness value is about 16 times of the substrate and is about 3 times of the PEO coating without any additive. Furthermore, the samples coated with graphene additive in the electrolytes displayed smallest standard deviation in the coatings micro-hardness measurements, which further illustrate the coatings uniformity.

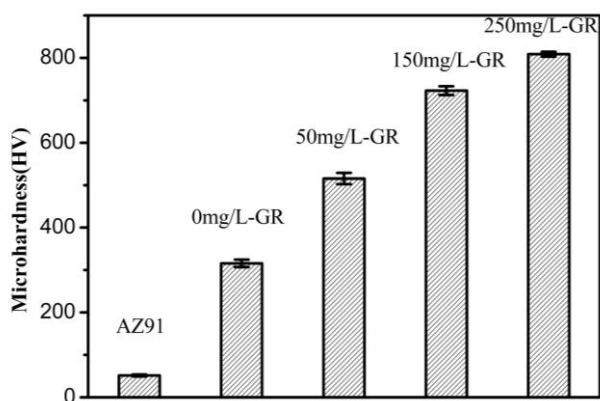


Figure 5. Microhardness of the PEO coatings processed in electrolytes added with different amounts of graphene

3.3 Microstructure and chemical compositions of the PEO coatings

Fig. 6 shows the SEM micrographs of the surface morphology of the PEO coatings processed in electrolytes containing different graphene additives. It could be observed that all coatings have similar characteristic, i.e. in the PEO coatings surfaces, there are always some micro-pores (Fig. 6a) and cracks (Fig. 6b). This is typical in surface morphology of the PEO coating reported in previous corresponding researches [5, 10, 39]. The gas bubbles extracting from the micro-discharge channels resulted in the formation of the micro-pores, and the cracks were formed by the thermal stress for the rapid solidification of the molten oxide in the relative cooling electrolyte [10,15,33]. Furthermore, the lower Pilling-Bedworth ratio (PBR) of magnesium may be also another reason of the high porosity of PEO coating on Mg alloys [40]. As can be seen from Fig. 6, the number and size of micro-pores in the coatings generated in the electrolytes containing graphene additive apparently reduced. Compared with the samples without graphene (Fig. 6a), there are some black substance embedded in the PEO coatings as indicated by the arrows in Fig. 6c. It is deduced the incorporation of graphene additive in the PEO coatings resulted in the darker color [28]. The inferring was supported by the EDS analysis of the chemical composition of the PEO coatings indicated by the box in Fig. 6d (Table 3) and the enlarge magnification of the black substance with EDS chemical composition analysis (Fig. 7). The EDS chemical composition analysis result indicates that the PEO coatings mainly contain elements of Mg, O, Si, Al and C, implying that the elements in the Mg alloy substrate and electrolyte are incorporated into the coating through PEO reaction. Especially, large amount of carbon was identified, indicating that the graphene additive in the

electrolyte was successfully incorporated into the PEO coatings. Fig. 7 obviously displays the graphene sheet embedded in PEO coating.

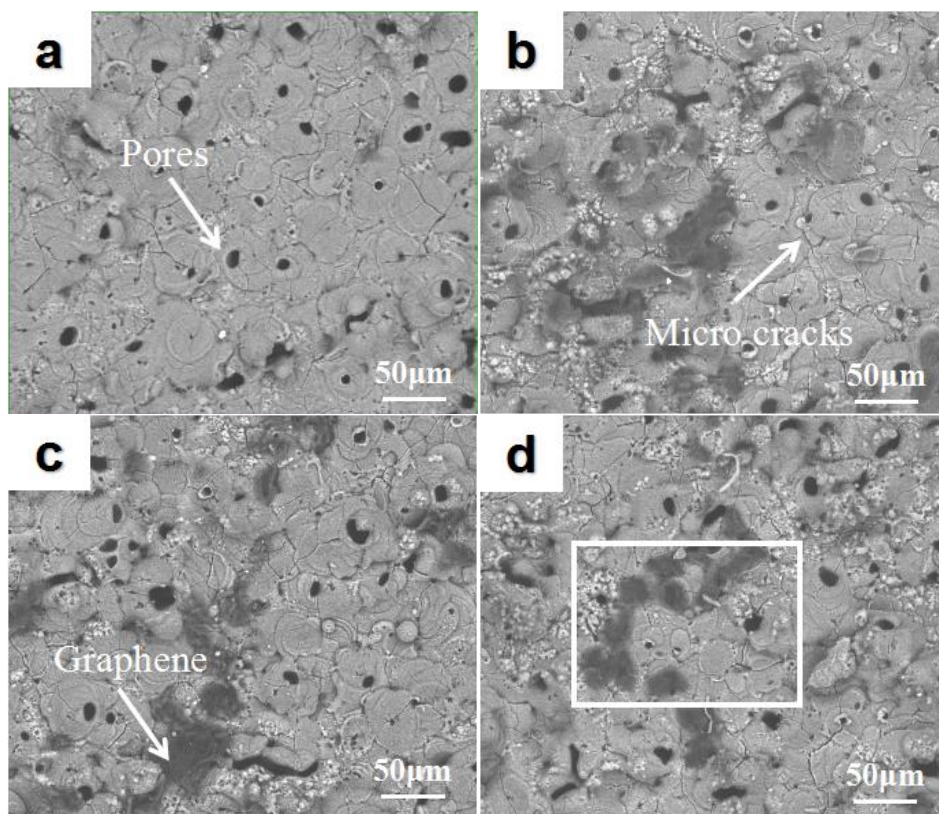
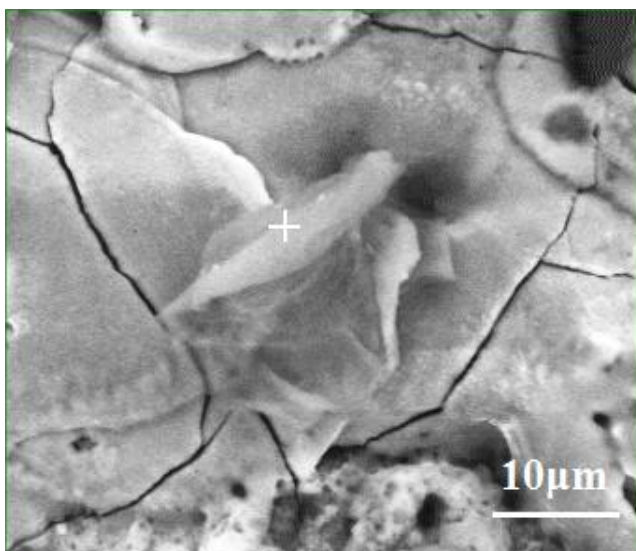


Figure 6. Surface morphology of the PEO coatings processed in electrolyte containing (a) 0, (b) 50 mg/L, (c) 150 mg/L and (d) 250 mg/L graphene additive

Table 3. Elemental contents (%) of the coatings marked by the box in Fig 6d.

Element	Mg	O	Si	Al	C
Wt. %	16.86	43.87	10.91	0.86	25.96
At.%	11.43	45.19	6.40	0.52	35.62

The cross section SEM images of the coatings processed in electrolytes added with different graphene additives were presented in Fig. 8. It shows that two main coating regimes existed in all coatings, i.e. an outer layer and an inner layer, which is typical in the cross section morphology for the PEO coatings [33,37,41-43]. It is obvious that the size and number of the micro-pores in PEO coating without (Fig. 8a) or less graphene absorbent (Fig. 8b) are larger, and its inner layers are thinner and looser, whereas the inner layer became denser and thicker, and the number and size of the micro-pores decreased (Fig. 8c,d) when the graphene additive in the corresponding electrolyte increased. It also could be found that there is no obvious discontinuity between the substrate and the PEO coating (Fig. 8d), indicating that the inner layer was integrated firmly with the substrate by sintered interlocking. So it is concluded that the graphene additive in the electrolyte during the PEO processing can reduce the porosity and conduce to obtain a more compact and uniform PEO coating.



Element	Wt%	At%
Mg	14.01	8.78
O	40.53	38.57
Si	5.96	3.23
Al	0.43	0.24
C	38.55	48.87

Figure 7. Enlarge magnification of the black substance and corresponding EDS chemical composition analysis result

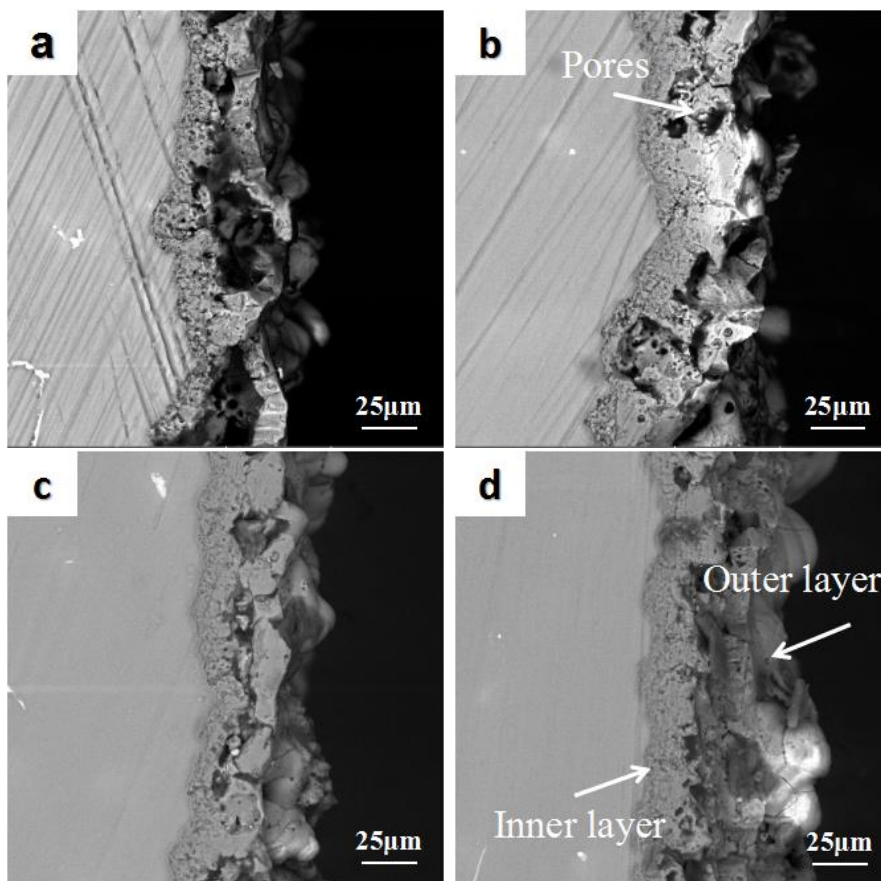


Figure 8. Cross section morphology of the PEO coatings processed in electrolyte containing (a) 0, (b) 50 mg/L, (c) 150 mg/L and (d) 250 mg/L graphene additive

3.4 Phase compositions of the PEO coatings

Fig. 9 discloses the phase compositions of the PEO coatings prepared in electrolytes containing different amount of graphene additives. The XRD spectra indicated that these PEO coatings are mainly consisted of Mg, MgO and Mg₂SiO₄ phases. As reported in reference [11,14,16], the Mg peaks in the diffraction in all coatings can be attributed to the penetration of X-ray through the PEO coatings. The MgO and Mg₂SiO₄ peaks are from the PEO coatings. Owing to the small amount incorporation and the number of graphene layers utilized in present investigation are fewer, there is no graphene signal detected in the XRD analysis.

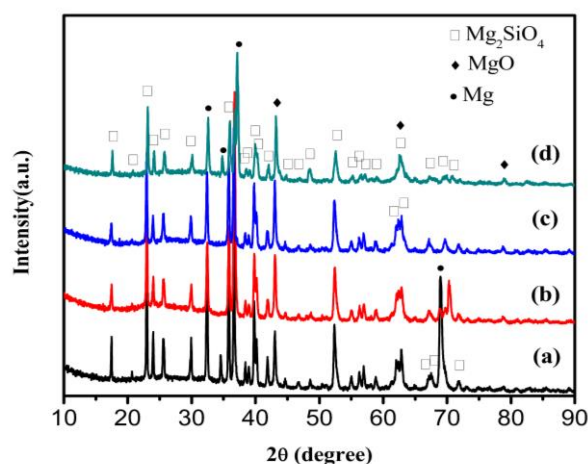


Figure 9. XRD phase analysis of the PEO coatings processed in electrolyte containing (a) 0, (b) 50 mg/L, (c) 150 mg/L and (d) 250 mg/L graphene additive

In order to further determine the graphene incorporation, as shown in Fig. 10, the X-ray photoelectron spectroscopy (XPS) was employed to determine the valence state of the elements in the PEO coating prepared in electrolyte containing 250 mg/L graphene additive. The detected XPS spectrum was fitted by the Gaussian function with Shirley background correction. Fig. 10a shows that the PEO coating comprise element of Si, O, Mg, and C. Notably, the signal of C 1s was detected in the coating. Although the identification of C 1s signal is common in the XPS surface scanning as hydrocarbons originated from the environment, the C 1s peak intensity in Fig. 10a was significantly stronger, which could be used as evidence of the graphene incorporation into the PEO coating [39]. In order to further identify the bonding state of the detected elements, the high resolution spectrum of the elements were fitted. The C 1s peaks (Fig. 10b) at 284.80eV, 286.29eV and 288.12eV are assigned as the sp² C-C bonding, the C-O bonding and C=O bonding, respectively [28], and the relative contents of the sp² C-C bonding, the C-O bonding and C=O bonding are listed in Table 4. The appearance of the C-O and C=O bonding is due to the high temperature during PEO processing and resulted in the oxidation of added graphene. The Mg 1s peaks (Fig. 10c) energies lie at 1303.00 eV, 1303.52 eV and 1304.00 eV for Mg, MgO and Mg₂SiO₄, respectively [44]. The Si 2p peaks (Fig. 10d) energy lies at 102.36 eV for Mg₂SiO₄ [45]. The O 1s peaks (Fig. 10e) energies lie at 532.43 eV, and 531.35eV for MgO and Mg₂SiO₄, respectively [46]. All the XPS peaks splitting results in Fig. 10 are acceptable based on the reason that

all identified peaks shift from the standard peaks below 1.0 eV. The XPS results conformed well with the XRD analysis result (Fig. 9).

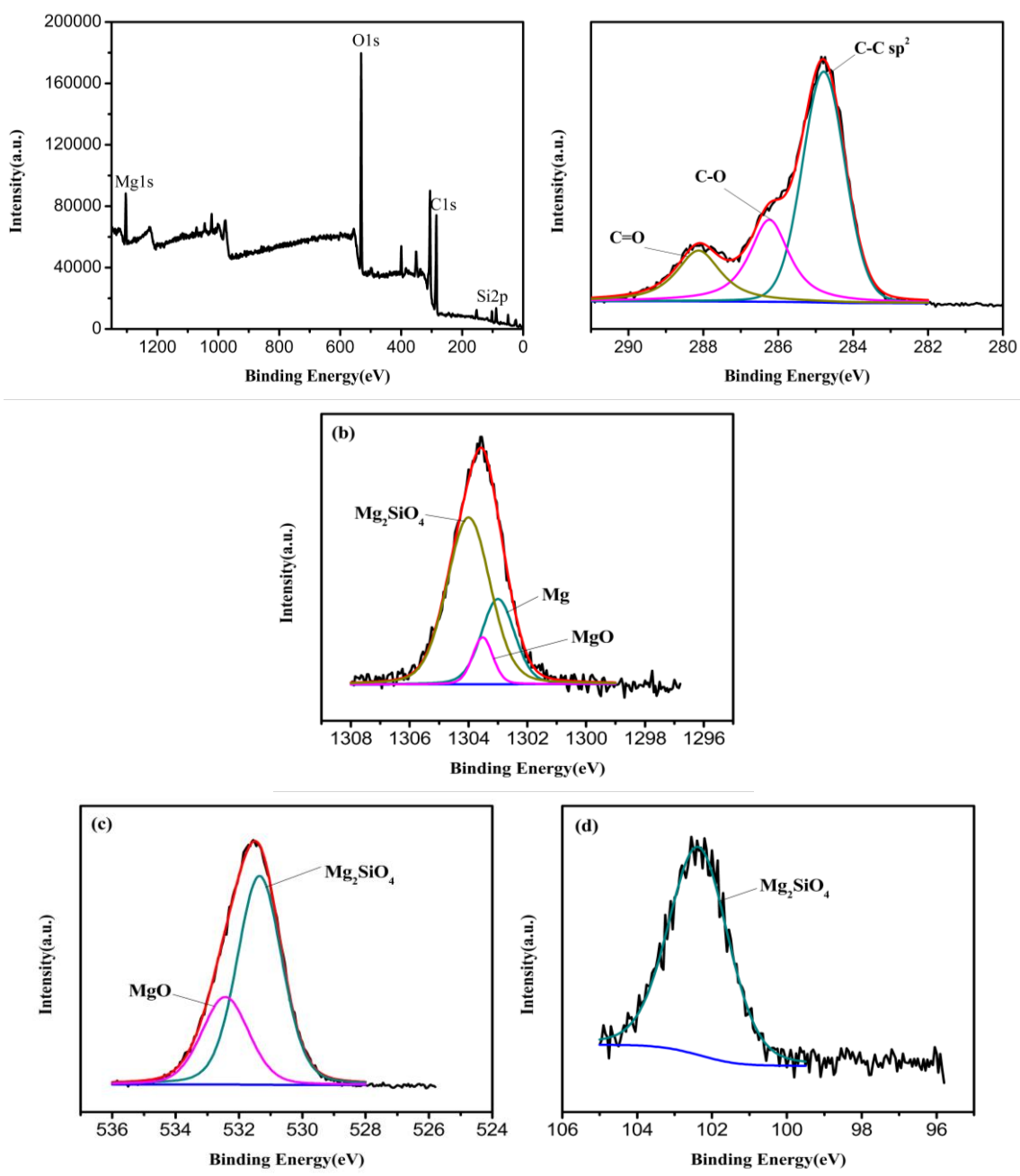


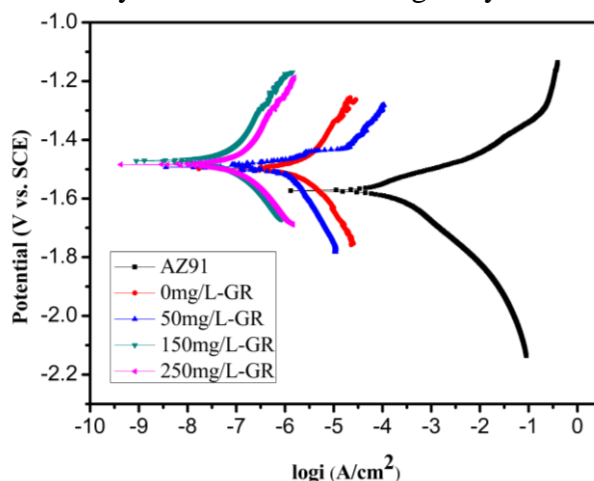
Figure 10. XPS spectra of the PEO coating processed in electrolyte containing 250 mg/L graphene additive. (a) the total spectrum, (b) the C 1s high resolution splitting spectrum, (c) the Mg 1s high resolution splitting spectrum, (d) Si 1s high resolution splitting spectrum and (e) O 1s high resolution splitting spectrum

Table 4. Atomic percentage of various group in PEO coating processed in electrolyte containing 250 mg/L graphene additive.

Functional group	sp ² C-C bonding	C-O bonding	C=O bonding
At. %	57.72	24.66	17.62

3.5 Electrochemical measurements

Effective electrochemical methods of potentiodynamic polarization and EIS technique were used to reveal the corrosion resistance of the coating. It is well known that the corrosion current density (i_{corr}), corrosion potential (E_{corr}) and Tafel slope are frequently used to evaluate the early stage corrosion resistance of the samples. For the polarization curves, the anodic curve is the important feature related to the corrosion resistance, while the cathodic reaction corresponding to the evolution of hydrogen [47,48]. Fig. 11 illustrates the potentiodynamic polarization curves of the blank AZ91 Mg alloy and the PEO coatings prepared in electrolytes containing different amount graphene additive. The electrochemical parameters derived by Tafel extrapolation method are summarized in Table 5. It could be found that current density decreased when the AZ91 Mg alloy coated with PEO coatings, and which indicates that the coatings restrain the anodic reaction and enhance the electrochemical stability. Among them, the blank AZ91 Mg alloy exhibits the lowest corrosion potentials (E_{corr}), highest corrosion current density (i_{corr}) and lowest Tafel slope. Especially, when 250 mg/L graphene was added into the electrolyte, the corrosion current density value of the PEO coatings is 1.15×10^{-7} A/cm², and decreased about 3 orders of magnitude relatively to the blank AZ91 Mg alloy.

**Figure 11.** Potentiodynamic polarization curves of the blank AZ91 Mg alloy and the samples with PEO coatings processed in electrolytes added with different amount of graphene

EIS measurements of the PEO coatings were conducted. Fig. 12 shows the Nyquist plots of the the blank AZ91 Mg alloy and the samples with PEO coatings processed in electrolytes containing different amount graphene additive. Fig. 12a shows that a capacitive semicircle at medium and high frequency and an induce semicircle at low frequency emerge in the Nyquist plot of blank AZ91 Mg alloy. The induce semicircle at low frequency imply that the AZ91 blank Mg alloy is easy corrosion in the aggressive solution. Whereas Fig. 12b shows that only one capacitive semicircle at medium and high

frequency emerge in the Nyquist plots for the PEO coatings, furthermore the capacitive semicircle radiuses are much larger than the blank AZ91 Mg alloy (Fig. 12a). The capacitive semicircle radius increased with increasing amount of graphene additive. Larger semicircle radius confirms higher corrosion resistance [26,49], therefore the PEO coating processed in electrolyte containing 250 mg/L graphene has the largest capacitive semicircle radius, indicating it is the most corrosion resistant.

Table 5. Tafel fitting results from the potentiodynamic polarization curves in Figure 11.

Sample	AZ91	0 mg/L GR	50 mg/L GR	150 mg/L GR	250 mg/L GR
Corrosion potential (E_{corr}) V	-1.5724	-1.4974	-1.4932	-1.4727	-1.4837
Corrosion current density (i_{corr}) A/cm ²	1.78×10^{-4}	2.09×10^{-6}	1.1×10^{-6}	8.32×10^{-7}	1.15×10^{-7}
Tafel slope b_a (mv/dec)	54	262	171	277	256
Tafel slope - b_c (mv/dec)	137	197	246	201	188

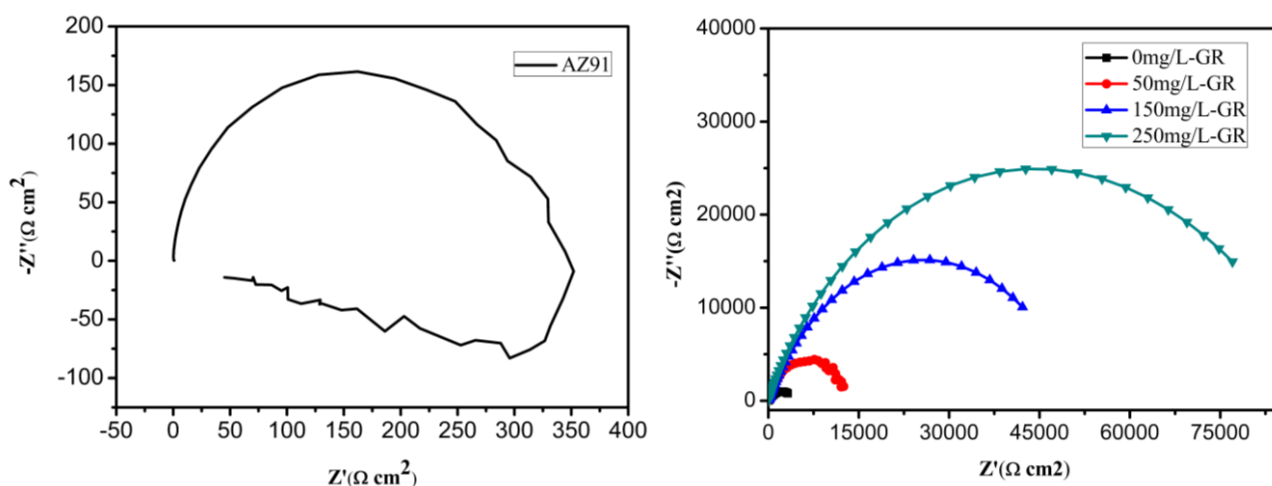


Figure 12. (a) Nyquist plots of the blank AZ91 Mg alloy and (b) Nyquist plots of the PEO coatings prepared in electrolyte containing different amount of graphene

Fig. 13 presents the Bode plots of the blank AZ91 Mg alloy and the PEO coatings with different amount of graphene additive in electrolyte. The corrosion mechanism and the robustness of the coating could be deduced from the analysis of the frequency behavior of the impedance [25]. Fig. 13 shows that in the range of low frequency (10^{-2} - 10^0 Hz), the total ($|Z|$) impedance of the blank sample is in the range of 10^1 - $10^2 \Omega\text{cm}^2$, whereas the impedance of the PEO coatings is up to $10^5 \Omega\text{cm}^2$. According to Reference [50] and [51], the lower frequency impedance is usually used to assess the coating's corrosion property and measure the inner layer performance. The apparently increasing in the impedance shows the increasing corrosion resistance.

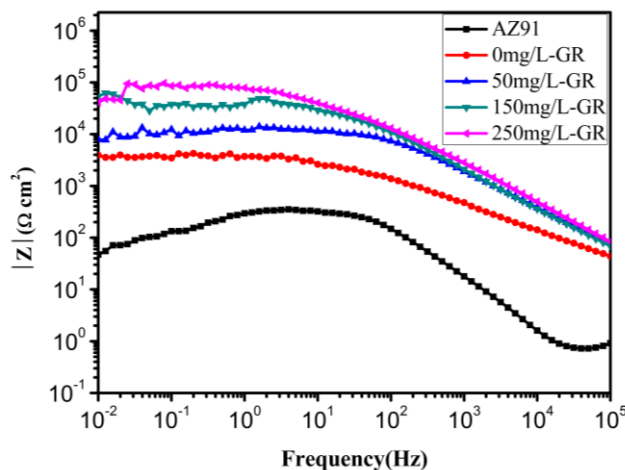


Figure 13. Bode plots in impedance form of the AZ91 Mg substrate and PEO coatings processed in electrolyte containing different graphene additive

Fig. 14 shows the equivalent circuit of the PEO coatings, in which the R_s , R_1 and R_2 refer to the electrical resistance of the solution, the outer layer and the inner layer, respectively. Furthermore, The CPE1 and CPE2 are constant phase elements corresponding to the outer layer and inner layer. The variation of equivalent circuit parameters was used to assess the coatings corrosion resistance. Table 6 summaries the equivalent circuits elements values, and n_p is a dispersion effect index close to 1. It can be seen that both R_1 and R_2 increased with increasing amount of graphene additive in electrolyte. A higher R_2 value imply higher corrosion resistance [28,52,53], therefore, when 250 mg/L graphene was added into the electrolyte, the PEO coating is the highest corrosion resistant.

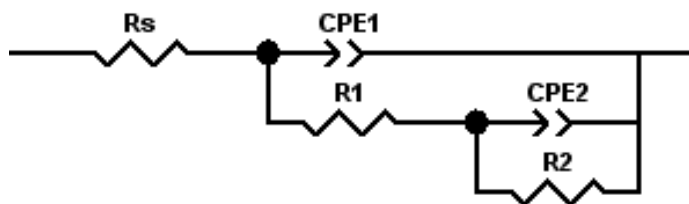


Figure 14. Equivalent circuit used for EIS spectra fitting

Table 6. The fitting electrochemical parameters of the PEO coatings

sample	R_s ($\Omega \text{ cm}^2$)	R_1 ($\Omega \text{ cm}^2$)	CPE1-T ($\Omega^{-1} \text{ S}^n \text{ cm}^{-2}$)	CPE1-P (n_i)	R_2 ($\Omega \text{ cm}^2$)	CPE2-T ($\Omega^{-1} \text{ S}^n \text{ cm}^{-2}$)	CPE2-P (n_i)
PEO	18.68	120.8	2.6656×10^{-7}	0.87387	4189	1.7181×10^{-5}	0.5435
50 mg/L-GR	24.88	3051	3.8965×10^{-8}	0.79364	10159	5.6735×10^{-7}	0.67353
150 mg/L-GR	28.43	6957	5.3622×10^{-7}	0.74321	44519	8.1336×10^{-7}	0.59261
550 mg/L-GR	12.03	18693	4.8631×10^{-7}	0.75337	75415	1.5185×10^{-6}	0.46499

The addition of graphene into the electrolyte during the PEO treatments of the AZ91 Mg alloy substrate could obviously improve the overall performance of the PEO coatings, which can be attributed

to the special structure and composition of the PEO coating with incorporation of graphene. As shown in Fig. 8, there are two main coating regimes visible existed the PEO coatings, i.e. an outer layer and an inner layer, which is typical in the cross section morphology for the PEO coatings [41-43]. It is obvious that the inner layer became denser and thicker, and the size and number of the micro-pores decreased when the graphene was added into the processing electrolyte. Therefore, the effect mechanism of graphene additives on the surface performance of PEO coating improvement can be schematically depicted as in Fig. 15. During the PEO processing, the graphene could grow into the coating, especially easily be embed in the inner layer, making the coating become more compact and thicker. This occurred because the graphene additive was preferentially located along the borders of the micro-pores and cracks in the PEO coating. When immersed in the corrosion medium, the graphene in the coatings would prevent the aggressive medium penetrating the inner layer, and then improve the corrosion resistance of AZ91 Mg alloy.

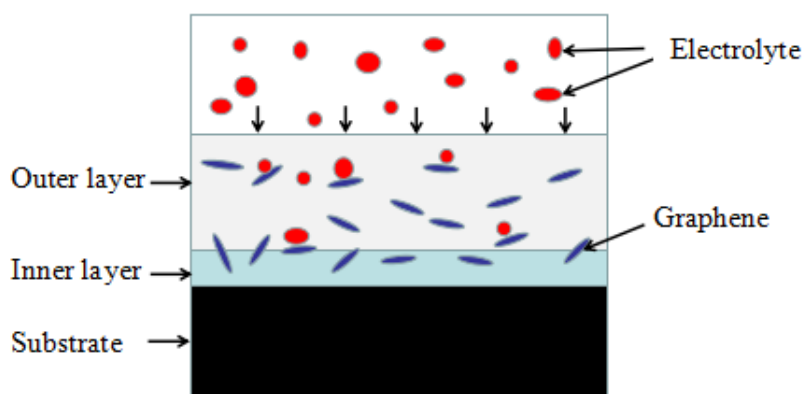


Figure15. Schematic depict of the anti-corrosion mechanism of the PEO coating with graphene incorporation

4. CONCLUSIONS

In present research, the method that adding the graphene into electrolyte to decrease the number and size of micro-pores in the PEO coating on AZ91 Mg was proposed. The microstructure and chemical composition analysis shows that the graphene can be incorporated into the PEO coating and decreased the number of micro-pores in the PEO coating. The electrochemical measurements and mechanical performance test demonstrate that the surface performance of the PEO coating was apparently improved upon the incorporation of graphene into the coatings. The micro-hardness of increased more than 15 times and the corrosion current was decreased by approximately three orders of magnitude when the graphene additive was 250 mg/L.

ACKNOWLEDGEMENTS

The authors acknowledge the support of the Ground Plan of Science and Technology Projects of Jiangxi Province (Grant No. KJLD2013078), the Open Project of Jiangxi Provincial Engineering Research

Center for Magnesium Alloys (Grant No. 201703) and Innovation and the Entrepreneurship Training Program for College Students of Gannan Normal University (Grant No. CX170050).

References

1. B.L. Mordike and T. Ebert, *Mater. Sci. Eng. A*, 302 (2001) 37.
2. M. Daroonparvar, M. A. Mat Yajid, N.M. Yusof, H.R. Bakhsheshi-Rad, E. Hamzah and H.A. Kamali, *J. Alloys Compd.*, 615 (2014) 657.
3. A. Apelfeld, B. Krit, V. Ludin, N. Morozova, B. Vladimirov and R.Z. Wu, *Surf. Coat. Technol.*, 322 (2017) 127.
4. L.J. Liu and M. Schlesinger, *Corros. Sci.*, 51 (2009) 1733.
5. X.J. Cui, M.T. Li, R.S. Song and Z.X. Yu, *Appl. Surf. Sci.*, 363 (2016) 91.
6. S. Pommiers, J. Frayret, A. Castetbon and M. Potin-Gautier, *Corros. Sci.*, 84 (2014) 135.
7. D.F. Zhang, Y.N. Gou, Y.P. Liu and X.X. Guo, *Surf. Coat. Technol.*, 236 (2013) 52.
8. H.T. Li, Q. Wang, M.H. Zhuang and J.J. Wu, *Vacuum*, 112 (2015) 66.
9. J. Lee, W. Chung, U. Jung and Y. Kim, *Surf. Coat. Technol.*, 205 (2011) 4018.
10. Gh. Barati Darband, M. Aliofkhaezraei, P. Hamghalma and N. Valizade, *J. Magnes. Alloys*, 5 (2017) 74.
11. M. Daroonparvar, M.A.M. Yajid, N.M. Yusof and H.R. Bakhsheshi-Rad, *J. Alloys Compd.*, 688 (2016) 841.
12. Z.P. Yao, P.F. Ju, Q.X. Xia, J.K. Wang, P. Su, H. Wei, D.Q. Li and Z.H. Jiang, *Surf. Coat. Technol.*, 307 (2016) 1236.
13. G. Rapheal, S. Kumar, N. Scharnagl and C. Blawert, *Surf. Coat. Technol.*, 309 (2017) 124.
14. H. Duan, C. Yan and F. Wang, *Electrochim. Acta*, 52 (2007) 3785.
15. H. Duan, K. Du, C. Yan and F. Wang, *Electrochim. Acta*, 51 (2006) 2898.
16. X. Lu, C. Blawert, M.L. Zheludkevich and K.U. Kainer, *Corros. Sci.*, 101 (2015) 201.
17. H. Nasiri Vatan, R. Ebrahimi-kahrizsangi and M. Kasiti-asgarani, *J. Alloy Compd.*, 683 (2016) 241.
18. X. Lu, M. Schieda, C. Blawert, K.U. Kainer and M.L. Zheludkevich, *Surf. Coat. Technol.*, 307 (2016) 287.
19. D.V. Mashtalyar, S.V. Gnedenkov, S.L. Sinebryukhov, I.M. Imshinetskiy and A.V. Puz, *J. Mater. Sci. Technol.*, 33 (2017) 461.
20. S. Stojadinović, N. Tadić, N. Radić, B. Grbić and R. Vasilić, *Surf. Coat. Technol.*, 310 (2017) 98.
21. R. Sanjinés, M.D. Abad, C. Vájuc, R. Smajda, M. Mionic and A. Megrez, *Surf. Coat. Technol.*, 206 (2011) 727.
22. A. A. Balandin, S. Ghosh, W. Bao, I. Calizo and D. Teweldebrhan, *Nano. Lett.*, 8 (2008) 902.
23. C. Lee, X. Wei, J. W. Kysar and J. Hone, *Science*, 321 (2008) 385.
24. Y. Tong, S. Bohm and M. Song, *Austin J. Nanomed. Nanotechnol.*, 1 (2013) 1003.
25. D. Prasai, J.C. Tuberquia, R.R. Harl, G.K. Jennings and K.I. Bolotin, *ACS Nano.*, 6 (2012) 1102.
26. M. Selvam, K. Saminathan, P. Siva, P. Saha and V. Rajendran, *Mater. Chem. Phys.*, 172 (2016) 129.
27. B.P. Singh, S. Nayak, K.K. Nanda, B.K. Jena, S. Bhattacharjee and L. Besra, *Carbon*, 61 (2013) 47.
28. J.M. Zhao, X. Xie and C. Zhang, *Corros. Sci.*, 114 (2017) 146.
29. S. Chen, A. Moore, W. Cai, J. Suk, J. An, C. Mishra, C. Amos, C. Magnuson, J. Kang, L. Shi and R. Ruoff, *ACS Nano*, 5 (2011) 321.
30. Z. Shi, M. Liu and A. Atrens, *Corros. Sci.*, 52 (2010) 579.
31. X.L. Zhang, Z.H. Jiang, Z.P. Yao, Y. Song and Z.D. Wu, *Corros. Sci.*, 51 (2009) 581.
32. E. McCafferty, *Corros. Sci.*, 47 (2005) 3202.

33. F. Wei, W. Zhang, T. Zhang and F. Wang, *J. Alloys Compd.*, 690 (2017) 195.
34. O. Khaselev, D. Weiss and J. Yahalom, *J. Electrochem. Soc.*, 146 (1999) 1757.
35. L.O. Snizhko, A.L. Yerkohin, A. Pilkington, N.L. Gurevina, D.O. Misnyankina, A. Leyland and A. Matthews, *Electrochim. Acta*, 49 (2004) 2085.
36. S. Ono, S. Moronuki, Y. Mori, A. Koshi, J. Liao and H. Asoh, *Electrochim. Acta*, 240 (2017) 415.
37. X. Lu, C. Blawert, Y. Huang, H. Ovri, M.L. Zheludkevich and K.U. Kainer, *Electrochim. Acta*, 187 (2016) 20.
38. A. Apelfeld, B. Krit, V. Ludin, N. Morozova, B. Vladimirov and R.Z. Wu, *Surf. Coat. Technol.*, 322 (2017) 127.
39. G. Lv, H. Chen, W. Gu, W. Feng, L. Li, E. Niu, X. Zhang and S. Yang, *Curr. Appl. Phys.*, 9 (2009) 324.
40. X. Zhou, G. E. Thompson, P. Skeldon, G. C. Wood, K. Shimizu and H. Habazaki, *Corros. Sci.*, 41 (1999) 1599.
41. J. Dou, G. Gu and C. Chen, *Mater. Lett.*, 196 (2017) 42.
42. J. Liang, P. B. Srinivasan, C. Blawert, M. Stormer and W. Dietzel, *Electrochim. Acta*, 54 (2009) 3842.
43. R. Arrbral, E. Matykina, F. Viejo, P. Skeldon, G.E. Thompson and M.C. Merino, *Appl. Surf. Sci.*, 254 (2008) 6937.
44. H.B. Yao, Y. Li and T.S. Wee, *Appl. Surf. Sci.*, 158 (2000) 112.
45. Y. Zhou, G. Pan, X. Shi, L. Xu, C. Zou, H. Gong and G. Luo, *Appl. Surf. Sci.*, 316 (2014) 643.
46. D.K. Aswai, K.P. Muthe, S. Tawde, S. Chodhury, N. Bagkar, A. Singh, S.K. Gupta and J.V. Yakhmi, *J. Crystal. Grow.*, 236 (2002) 661.
47. C. Gu, J. Lian, J. He, Z. Jiang and Q. Jiang, *Surf. Coat. Technol.*, 200 (2006) 5413.
48. X. Cui, Y. Li, Q. Li, G. Jin, M. Ding and F. Wang, *Mater. Chem. Phys.*, 111 (2008) 503.
49. M. Mandal, A.P. Moon, G. Deo, C.L. Mendis and K. Mandal, *Corros. Sci.*, 78 (2014) 172.
50. S.V. Lamaka, M.F. Montemor, A.F. Galio, M.L. Zheludkevich, C. Tridade, L.F. Dick and M.G.S. Ferreira, *Electrochim. Acta*, 53 (2008) 4773.
51. S.C. Chuang, J.R. Cheng and H.C. Shih, *Corros. Sci.*, 42 (2000) 1249.
52. H. Ma, D. Li, C. Liu, Z. Huang, D. He, Q. Yan, P. Liu, P. Nash and D. Shen, *Surf. Coat. Technol.*, 266 (2015) 151.
53. M. Ren, S. Cai, T. Liu, K. Huang, X. Wang, H. Zhao, S. Niu, R. Zhang and X. Wu, *J. Alloys Compd.*, 591 (2014) 34.